Disorder-Enhanced Dimensionless Thermoelectric Figure of Merit zT of Non-stoichiometric Organic Conductor (TTT)2I3+δ (δ ≤ 0.1)

AUTHOR(S):

Yoshino, Harukazu; Hasegawa, Akifumi; Kuroda, Natsuki; Ishikawa, Manabu; Tanaka, Rika; Kozaki, Masatoshi; Nakano, Yoshiaki; Otsuka, Akihiro; Yamochi, Hideki

CITATION:

Yoshino, Harukazu ...[et al]. Disorder-Enhanced Dimensionless Thermoelectric Figure of Merit zT of Non-stoichiometric Organic Conductor (TTT)2I3+δ (δ ≤ 0.1). Journal of the Physical Society of Japan 2019, 88(10): 104708.

ISSUE DATE:

2019-09-24

URL:

http://hdl.handle.net/2433/244163

Disorder-Enhanced Dimensionless Thermoelectric Figure of Merit zT of Non-stoichiometric Organic Conductor $(TTT)_2I_{3+\delta}$ ($\delta \leq 0.1$)

Harukazu Yoshino[1]*, Akifumi Hasegawa[1], Natsuki Kuroda[1], Manabu Ishikawa[2], Rika Tanaka[3], Masatoshi Kozaki[1], Yoshiaki Nakano[2,4], Akihiro Otsuka[2,4], and Hideki Yamochi[2,4]

[1]*Graduate School of Science, Osaka City University, Sumiyoshi-ku, Osaka 558-8585, Japan*
[2]*Research Center for Low Temperature and Materials Sciences, Kyoto University, Sakyo-ku, Kyoto 606-8501, Japan*
[3]*Graduate School of Engineering, Osaka City University, Sumiyoshi-ku, Osaka 558-8585, Japan*
[4]*Graduate School of Science, Kyoto University, Sakyo-ku, Kyoto 606-8502, Japan*

Sample dependence of dimensionless thermoelectric figure of merit (zT) and power factor (PF) were determined for the non-stoichiometric organic conductor $(TTT)_2I_{3+\delta}$ (TTT = tetrathiatetracene, $\delta \leq 0.1$) with the simultaneous measurement of the electrical resistivity (ρ), thermopower (S) and thermal conductivity on small single crystals. Both the zT and PF show large sample dependence between 10 and 310 K, even though all the samples have nearly stoichiometric composition of TTT:I_3^- ~ 2:1 ($\delta \sim 0$). It was found that both the electrical conductivity ($\sigma = 1/\rho$) and S increase at room temperature as disorder — that is phase mismatch among the iodine chains — becomes more pronounced. This behavior contrasts the usual tendency that the S decreases as the σ increases in conventional conductors; and suggests a new strategy to improve the zT and PF by introducing an appropriate type of disorder.

1. Introduction

Thermoelectric materials directly convert low-grade thermal energy to useful electricity. Their performance is often evaluated by the power factor $PF = \sigma S^2$ and the dimensionless thermoelectric figure of merit zT,

$$zT = \frac{\sigma S^2}{\kappa} T = \frac{PF}{\kappa} T. \quad (1)$$

*yoshino@sci.osaka-cu.ac.jp

Here σ, S and κ denote the electrical conductivity, thermopower (Seebeck coefficient) and thermal conductivity at a temperature T. The PF reflects the ability of power generation, while the zT represents the efficiency of conversion from heat to electricity.

For practical purposes, $zT > 1$ is a kind of the lowest limit; and even $zT > 3$ in a wide temperature range is required for thermoelectric materials to compete with other energy-generation technologies.[1] To achieve such high zT is, however, very difficult since, for example, a material with higher σ usually shows higher κ and smaller S. Thus one needs a strategy to manage such contradictory requirements.

The title compound $(TTT)_2I_{3+\delta}$ ($\delta \leq 0.1$, TTT = tetrathiatetracene, Fig. 1) is a quasi-one-dimensional (Q1D) organic molecular conductor made of the segregated stacks of the TTT donor molecules and iodine (I_3^-) chains parallel to the most conducting $\boldsymbol{b}$-axis.[2–6] It is known that its σ along the $\boldsymbol{b}$-axis — up to 1000 S·cm^{-1}or even more — is the highest of molecular conductors at room temperature.[7–12]

Casian *et al.* theoretically pointed out the possibility of obtaining rather large zT (> 2) by tuning the band filling of $(TTT)_2I_{3+\delta}$,[13–15] which is abbreviated as TTT–I_3 below. Huewe *et al.*, however, reported the experimental zT of TTT–I_3 amounts to only 0.03 — it is far below the theoretical expectation — at room temperature.[16]

TTT–I_3 is, however, known to exhibit large sample dependence of physical properties due to its non-stoichiometric nature.[2,8,10–12,17,18] For example, a chemical analysis showed that the δ of iodine content $(3 + \delta)$ changes between 0 and 0.1,[17] while the crystal density measurement implied that the δ scatters around 0.02; and some crystals might have even a minus value of δ.[10]

In addition, the sample dependence is due not only to the δ but also to the disorder observed as diffuse sheets perpendicular to the $\boldsymbol{b}$-axis in X-ray diffraction.[2,6,11,12,19,20] The disorder reflects the uncorrelated phases among iodine chains and its degree changes from sample to sample as well as temperature.

Thus, in this paper, we studied the sample dependence of zT and PF to find the condition

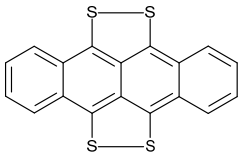

TTT

Fig. 1. Structural formula of TTT.

Table I. Original size of samples of $(TTT)_2I_{3+\delta}$.

sample	
A (#1602)	$0.90 \times 0.060 \times 0.084$ mm^3
B (#1704)	$1.48 \times 0.098 \times 0.036$ mm^3
C (#1701)	$0.48 \times 0.070 \times 0.034$ mm^3

of achieving higher performance of this potential candidate of the molecular thermoelectric material. In combination with the X-ray diffraction measurements, it has been revealed that the disorder basically governs the sample dependence of the transport properties, while almost no change in the δ has been observed for the present samples.

As reported previously, it was observed that the disorder enhances the σ at room temperature. The most remarkable thing of the present results is that the S also increases as the σ becomes higher. The tendency is completely opposite to that observed for conventional electrical conductors; and provides a potentially new strategy to improve the zT by introducing an appropriate type of disorder.

2. Experimental

The sample preparation and transport measurements were carried out at Osaka City University (OCU). Black needle-like single crystals of TTT–I_3 were grown in the nitrobenzene solution of TTT and I_2 with slow cooling from 100 °C to room temperature for about 20 days.[21)]

The X-ray diffraction analysis — also carried out at OCU[22)] — confirmed the same type of crystal structure as reported.[2–6)] The analysis could not be, however, completed due to existence of the diffuse sheets along the $\boldsymbol{a}^*\boldsymbol{c}^*$ plane at room temperature. This shows that the iodine chains are uncorrelated with one another.[2)] Note that the chain direction is taken not as the $\boldsymbol{b}$-axis but as the $\boldsymbol{c}$-axis in some literature.[2,4,5)]

The electrical resistivity ρ, thermopower (Seebeck coefficient) S and thermal conductivity κ were simultaneously measured on each single crystal in Table I to determine zT and PF. Figure 2 shows a schematic view of our sample holder to measure the ρ, S and κ of a small ($\sim$ 1 mm) sample simultaneously. The three samples are all that we could complete the transport measurements since it is rather difficult to make all wiring on a sample without any damage.

The both ends of the sample (a) were attached to an annealed gold wire (b, 100 μm in diameter, Tanaka Kikinzoku) and the Manganin wire (c, 100 μm in diameter, Nilaco) with carbon paste (Fujikurakasei XC-12), respectively. The other end of the gold wire was con-

nected onto the gold deposited surface of a large copper block (d1) with silver paste (DuPont 4922); the gold wire supported the sample and Manganin wire above the block with a gap of ~ 2 mm. Another annealed gold wire (e, 10 μm in diameter, Tanaka Denshi Kogyo) was used to connect the Manganin wire (with carbon paste) to a small copper block (d2) (with silver paste) electrically.

The contact points of two pairs of Chromel–Constantan thermocouples (f1 and f2) were attached to the sample with carbon paste. Similarly the contact points of other two thermocouples (f3 and f4) were done so to the Manganin wire. The open ends of these thermocouples were connected to the solder-coated ends of eight copper wires (g) with silver paste. The copper wires coated with polymer were glued to the surface of the d1 copper block with varnish to achieve the good thermal contact to the resistance thermometer (h) measuring the temperature of the contacts between the thermocouples and the copper wires on the block.

Finally, the contact point of the last thermocouple (f5) was attached to the right end of the Manganin wire with epoxy resin. This thermocouple worked as a heater, to which DC electrical current was supplied via two small copper blocks (d3 and d4). Joule heat as well as positive Peltier heat were supplied to the Manganin wire with the appropriate direction of DC current.

The ρ was measure by the DC four-terminal method. The electrical current I_s was supplied through d1, b, a, c, e and d2 as in Fig. 2. Then the DC voltage was measured using each Chromel leg of f1 and f2.

The temperature gradient along the Manganin wire and sample was generated by applying the heat current I_q with the heater, while the I_s was turned off. After the steady state was achieved, the temperature differences on the sample and Manganin was determined by the thermocouples. The κ of the sample was determined relative to that of Manganin.[23)]

At the same time, the thermoelectric powers were measured between the Chromel legs as well as between the Constantan legs of f1 and f2, respectively. Then the thermopower S was determined by the so-called direct method.

There are three major paths of heat leak giving overestimated κ; namely, the leaks 1) through the remaining air around the sample holder, 2) through the thermocouples, and 3) by radiation loss above 200 K, respectively.

To suppress the influence of the remaining air, the sample holder was placed in a vacuum chamber. The inside pressure was monitored by an ionization vacuum gage; it indicated less than 10^{-10} Pa during the measurement. To suppress the leak through the thermocouples, we used the thinnest thermocouple wires (12.7 μm in diameter, Omega) commercially avail-

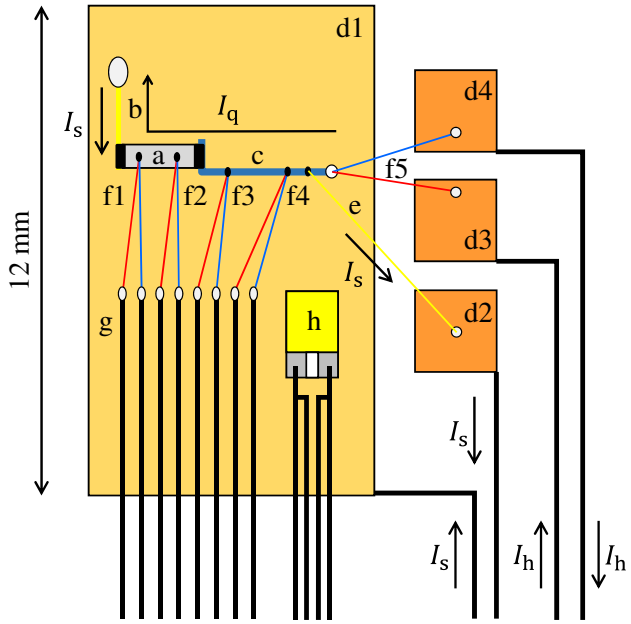

Fig. 2. (Color online) Schematic of the sample holder for measuring thermal conductivity. a - sample, b - thick gold wire, c - Manganin wire, d1–d4 - copper blocks, e - thin gold wire, f1–f5 - Chromel–Constantan thermocouples, g - copper leads, h - resistance thermometer.

able. The effect of radiation is difficult to suppress in the present measurement. Despite these difficulties, the magnitude and overall temperature dependence of the κ is very close to that reported before.[16] We will discuss the accuracy of the κ later.

To determine ρ and κ, we used the cross-sectional area A_S; and the thermocouple distance L_S regarding each crystal as a cuboid. Note that each of A_S and L_S appears twice from ρ and κ in $zT = S^2T/(\rho\kappa)$ and cancels in the denominator with each other. Thus we can neglect the ambiguities from the sample dimensions in determining zT.

The present measurements are essentially the same as described in literature.[24,25]

After measuring the transport properties, we examined the iodine content in each crystal by X-ray diffraction measurement at Kyoto University. The gold-evaporated parts of the three samples (#1602, #1701, and #1704) were cut out before the measurement, and the size of the crystals was reduced to $0.26 \times 0.08 \times 0.06$ mm^3, $0.27 \times 0.07 \times 0.04$ mm^3 and $0.20 \times 0.10 \times 0.04$ mm^3, respectively.

The X-ray diffraction images were accumulated by Bruker SMART Apex II CCD diffractometer with graphite monochromatized Mo Kα radiation (50 kV, 30 mA) at 85–300 K under nitrogen gas flow. To obtain the diffuse scattering image without detector saturation, the exposure time was set to 100 sec, whereas the oscillation angle of 0.25° was adopted to reduce

the background level. The accumulated photographs in the full sphere experiment were processed by Bruker Apex3 program to generate the precession images utilizing the similar unit cell parameters reported by Lowe-Ma *et al.* with *Cmca* (*Cmce*) space group.[6)]

3. Results

3.1 Iodine content and disorder

Hilti and Mayer reported the determination of δ using the difference in periods of TTT (b) and I_3^- (b') chains.[2)] Here b is the distance between neighboring TTT molecules; and $b' \simeq 2b$ corresponds to the period of the I_3^- unit, respectively. The δ is zero when $b' = 2b$, while b' becomes shorter than $2b$ for $\delta > 0$.

Figure 3 shows the precession images of X-ray diffraction at room temperature for the samples #1602, #1704, and #1701, respectively. The layer lines corresponding to $b' \simeq 9.9$ Å were observed by rotating the crystals around the $\boldsymbol{b}$-axis. The overall feature of the layer lines is similar to that reported before.[6,11,17,19,20)]

The continuous diffuse scattering in the layer lines, two of which at $k' = \pm 3$ are the most pronounced, indicates the weak correlation of the I_3^- arrangements in the $\boldsymbol{ac}$ plane. Since the Bragg spots originating from the TTT lattice are overlapping with the diffuse lines from the I_3^- one, the compositions of our crystals are concluded to have TTT:I_3^- = 2:1 within the experimental errors.[2)]

It should be noted that the Bragg spots from the TTT lattice should overlap with the diffuse lines from the I_3^- one only at even k' since $b' \simeq 2b$. The clear spots at $k' = \pm 3$ suggest that the TTT lattice is modulated by the I_3^- one and the real period of the former is doubled.[6)]

On the other hand, it was found that the observed diffuse lines are most pronounced for the #1602, while the least for #1701. It means that the sample #1602 is the most disordered or, in other words, it has the most uncorrelated iodine chains of the three. Below we call #1602, #1704 and #1701 the samples A, B, and C according to the degree of disorder.

3.2 Electrical resistivity

Figure 4(a) shows the temperature dependence of ρ. The overall temperature dependence is similar to that reported before.[11,12)] At 300 K the $\sigma = 1/\rho$ is 1400, 1000, and 840 S·cm^{-1} for A–C, respectively. Namely, a more disordered sample has a higher σ and this relation is consistent with that reported by Khanna *et al.*[11)]

Below 300 K the ρ is weakly metallic, but gradually turns into semiconducting. The temperatures of the resistivity minimum T_{min}, where a numerical derivative becomes zero

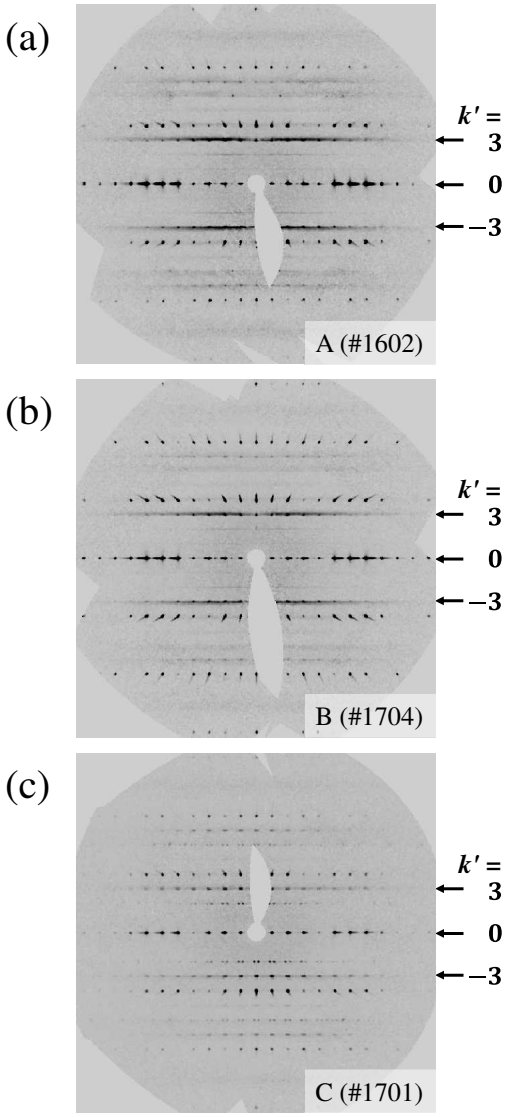

Fig. 3. Room-temperature X-ray patterns of ($hk0$) observed for the $(TTT)_2I_{3+\delta}$ samples (a) A (#1602), (b) B (#1704), and (c) C (#1701), respectively. The horizontal arrows indicate the Bragg spots from the TTT lattice overlappong with the diffuse lines of $k' = -3,\ 0,\ 3$ from the iodine chains.

(Fig. 4(b)), are determined as 90, 95 and 120 K for A–C, respectively. These T_{min}'s correspond to "low-" or "middle-quality" samples reported by Hiliti and Mayer.[2)] Again the relation between the sample quality (disorder) and T_{min} corresponds to that reported before.

Below about 50 K the ρ starts to increase rapidly with lowering temperature due to a metal-to-insulator (M–I) transition[11,12,17,26)] or localization caused by the iodine disorder.[8,27)] The transition temperature T_{M-I} determined as the peak center in Fig. 4(b) is about 41, 44, and 41 K for A, C, and B, respectively.

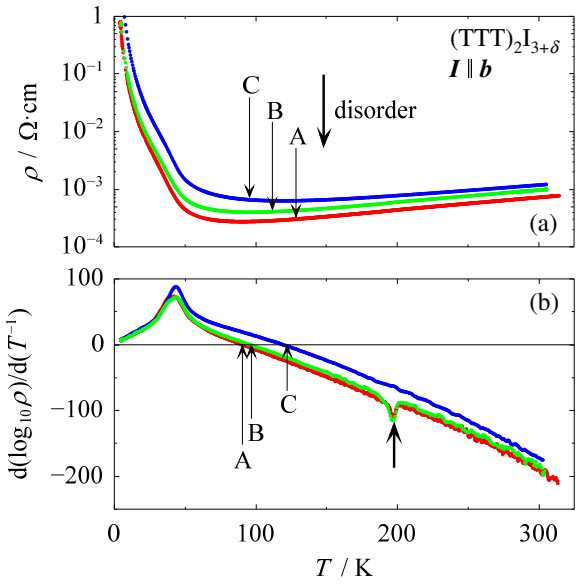

Fig. 4. (Color online) (a) Temperature dependence of the electrical resistivity of $(TTT)_2I_{3+\delta}$ for the samples A (red), B (green), and C (blue). (b) Numerical derivative of the Arrhenius plot of the same data in (a). The thick arrow at 197 K indicates anomalies associated with a phase transition.

Besides the M–I transition, another change was found as an anomaly in the derivative at 197 K (the thick arrow in Fig. 4(b)). It was observed for A and B, but not for C. Megtert reported that, for one sample of TTT–I_3, the diffuse sheets in X-ray diffraction at room temperature progressively change into spots.[20] This is also the case with another sample from the same batch as the present ones. The change in the diffuse sheets suggests that the correlation between neighboring iodine chains develops on cooling. The newly found anomaly at 197 K seems to imply such a structural change also includes a discontinuity in addition to the progressive temperature variation.

3.3 Thermopower

Figure 5 shows the temperature dependence of the S in the whole (a) as well as in an enlarged scales (b), respectively. On cooling, the S is metallic below 310 K and turns to non-metallic below about 50 K. The values at 300 K are 50, 49 and 47 $\mu V \cdot K^{-1}$ for A–C, respectively. Data scattering of the S was slightly larger for B than for the others above 50 K, but its standard deviation amounts to only 0.04 $\mu V \cdot K^{-1}$ at room temperature. Namely, the sample dependence is very clear even in the metallic region. The absolute S increases as the disorder develops at room temperature (Fig. 5(b)).

The sample dependence becomes much more distinct below 50 K. The S increases rapidly

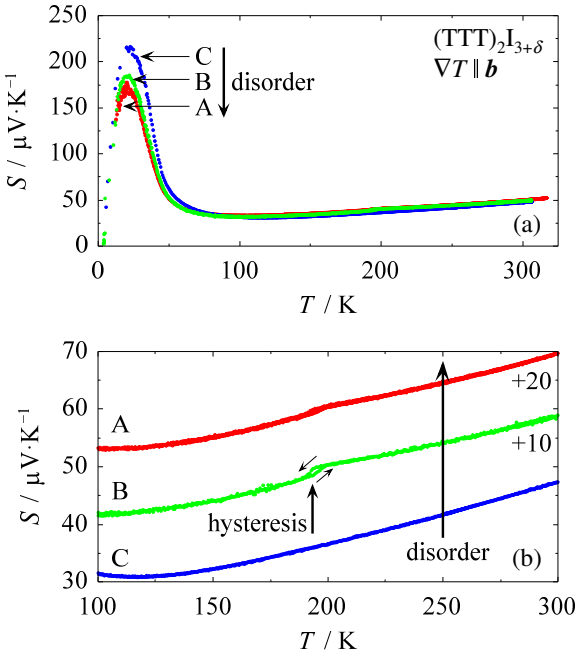

Fig. 5. (Color online) (a) Temperature dependence of the thermopower of $(TTT)_2I_{3+\delta}$ for the samples A (red), B (green), and C (blue). (b) The same data in (a) in an enlarged scale. The data for A and B are shifted by +20 and +10 μV·K^{-1}, respectively. The thick up arrow indicates the anomaly associated with a phase transition.

and reaches its maximum, 170, 185 and 210 μV·K^{-1} at 20 K for A–C, respectively, while the data points are rather scattered due to the large sample resistance in the non-metallic region. Note that the relation between the disorder and S at 20 K is opposite to that at 300 K.

The overall behavior of the present S is very similar to that reported before.[11,12,26] Khanna *et al.* claimed that the peak height at 20 K decreases from about 270 μV·K^{-1} of the least-disordered samples to 40 μV·K^{-1} of the highly-disordered ones. The present samples correspond to the "medium-disordered" ones in the literature

At 300 K, however, the relation between the disorder and absolute S does not show simple correspondence to the previous result. Khanna *et al.* claimed that the disorder suppresses the S, while it is opposite in the present case. We will discuss this apparent contradiction later.

On the other hand, a hysteretic anomaly was observed just below 200 K for A and B (Fig. 5(b)). The temperature of the anomaly in the S exactly corresponds to that in the derivative of the ρ (Fig. 4(b)). The hysteresis strongly suggests the existence of a first-order phase transition never reported before.

It should be emphasized that the observed hysteresis is not spurious one caused by the different sweep directions of temperature with a rapid rate. For example, for B in this temper-

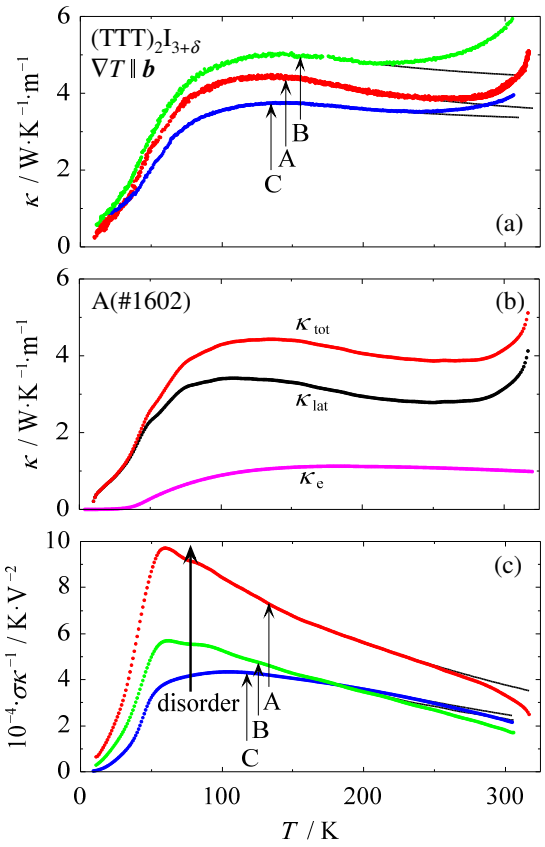

Fig. 6. (Color online) (a) Temperature dependence of the thermal conductivity of $(TTT)_2I_{3+\delta}$ for the samples A (red), B (green), and C (blue). Black solid curves are extrapolations of the data below 200 K to higher temperatures. (b) Rough estimates of the lattice and electronic thermal conductivities κ_{lat} (black) and κ_e(pink) of A, the latter of which was estimated by assuming Wiedemann–Franz law. (c) The ratio of the electrical conductivity to thermal conductivity σ/κ.

ature range, the sweep rate was ±10 K·hour^{-1} with sampling period less than 5 min; the temperature difference to determine the S was about 0.5 K, while the transition width seems to be about 4 K. The reason why such an anomaly was not reported in the previous works[8,11,12,16,26] is likely due to rough data interval and/or because their samples are similar to C.

3.4 Thermal conductivity

Temperature dependence of the κ (Fig. 6(a)) is very weak above 100 K and the values are almost within 4 ± 1 W·K^{-1}·m^{-1} for all the samples. Note that the upturn above 200 K is due to the radiation loss of heat. Black solid curves are extrapolation of the data between 175 and 200 K to higher temperatures by fitting a function $\kappa(T) = c_0 + c_1/T$, where c_0 and c_1 are fitting parameters. The overall behavior is very similar to that determined by the thermal-diffusivity measurement.[16]

In addition to the radiation, the heat leak through the thermocouples is unavoidable in the whole temperature region. This results in an overestimate, which depends on the dimensions of a sample and a reference as well as length of thermocouples. Therefore, the accuracy of the absolute values of κ is not so good as compared with that of the ρ and S. Nevertheless, the curves in Fig. 6(a) are very similar to one another suggesting the small sample dependence of the κ.

Figure 6(b) shows the rough estimates of the lattice (κ_{lat}) and electronic (κ_{e}) thermal conductivities of A. The κ_{e} was calculated from the $\rho = 1/\sigma$ in Fig. 4(a) assuming the Wiedemann–Franz law,

$$\kappa_{\mathrm{e}} = L_0 \sigma T, \tag{2}$$

with the Lorenz number $L_0 = 2.44 \times 10^{-8}$ W·Ω·K^{-2}. The κ_{lat} was obtained by subtracting the κ_{e} from the smoothed data of the total thermal conductivity $\kappa_{\mathrm{tot}}(= \kappa)$ of A. The ratio of the κ_{lat} to κ_{e} is about 3 in the metallic region. This is also the case with the samples B and C.[28] Namely, the lattice contribution seems dominant in the temperature dependence of the κ.

This is also shown by comparing the σ/κ as in Fig. 6(c). The errors in determining sample dimensions are included in each of the κ and σ in the same manner, but they are canceled in the σ/κ, while the influence of the heat leaks is still remaining. Again, the large differences in the absolute values and shapes of the curves in Fig. 6(c) clearly show the substantial contribution of the lattice to the heat conduction since the electronic component κ_{e} should be scaled by the σ at each temperature.

The large sample dependence of the σ/κ is caused by the σ, while that of the κ remains small due to the small change in the dominating κ_{lat}. This explains the major part of the sample dependence of the zT and PF as shown below.

3.5 zT and PF

The $zT = \sigma S^2 T/\kappa$ and $PF = \sigma S^2$ of TTT–I_3 are calculated by combining the data in Figs. 4(a), 5(a), and 6(a) after smoothing them.

The highest zT (Fig. 7(a)) is 0.025 at 290 K observed for A, but it will reach 0.029 at 300 K, if the upturn of the κ can be corrected as in Fig. 6(a). This is very close to that reported by Huewe *et al.*[16] The zT of the other samples B and C is almost a half of A.

The zT has a peak at about 35 K, which is higher than that of the S at 20 K and rather close to that of the derivative of ρ at 40 K. This is also the case with the PF (Fig. 7(b)). The peak values of PF range from 390 μW·K^{-2}·m^{-1} for C to 730 μW·K^{-2}·m^{-1} for A. Above 100 K, the

Table II. Typical values of zT, PF, σ, S, and κ of $(TTT)_2I_{3+\delta}$.

	T [K]	zT	PF [$\mu W \cdot K^{-2} \cdot m^{-1}$]	σ [$S \cdot cm^{-1}$]	S [$\mu V \cdot K^{-1}$]	κ [$W \cdot K^{-1} \cdot m^{-1}$]
A (#1602)	35	0.019	7.3×10^2	5.9×10^2	1.1×10^2	1.4
	290	0.025	3.4×10^2	1.5×10^3	49	4.0
	300	0.028*	3.4×10^2	1.4×10^3	50	3.7*
B (#1704)	35	0.012	6.0×10^2	4.0×10^2	1.2×10^2	1.7
	300	0.013	2.5×10^2	1.0×10^3	49	5.7
C (#1701)	35	0.011	3.9×10^2	1.5×10^2	1.6×10^2	1.3
	300	0.015	1.9×10^2	8.4×10^2	47	3.8

* Values roughly corrected the enhancement of the thermal conductivity κ due to the heat radiation.

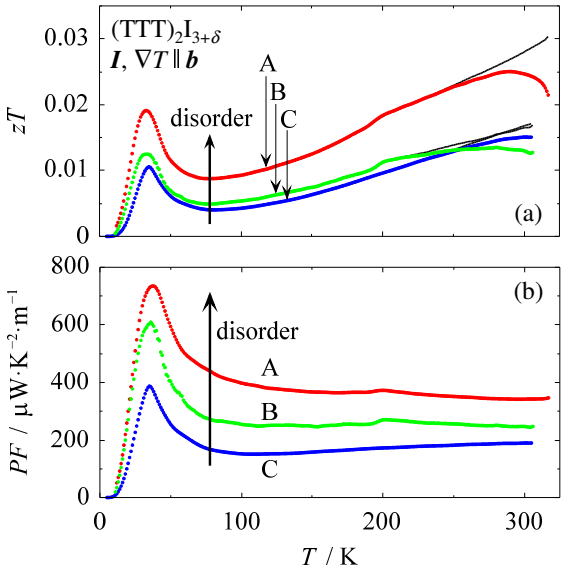

Fig. 7. (Color online) (a) Dimensionless thermoelectric figure of merit zT and (b) power factor PF of $(TTT)_2I_{3+\delta}$ for the samples A (red), B (green), and C (blue). Black solid curves in (a) are the extrapolation of the data below 200 K to higher temperatures.

PF remains almost constant because of the compensation of the increasing S and decreasing σ. Thus the increasing zT in the metallic region is mostly attributed to the temperature factor in eq. (1) since the κ is nearly constant.

There is a tendency that the zT and PF are higher for more disordered samples except for the zT of B and C near room temperature (Fig. 7(a)). We will discuss this below.

The typical values of the transport parameters are summarized in Table II for all the three

samples studied.

4. Discussion

4.1 Origin of sample dependence

As shown in the previous section, the sample dependence of zT and PF is not due to the change in δ but due to the disorder. Namely, more uncorrelated iodine chains seem favorable for higher zT and PF in TTT–I_3.

Disorders usually suppress the electrical conductivity of metals by increasing the scattering probabilities of electrical carriers. In TTT–I_3, however, when the iodine chains become more correlated or ordered to one another, intermodulation of TTT and iodine chains occurs.[6,20] It will result in complex band folding and lowering the σ.

Effect of the disorder on the thermopower seems different at low and high temperatures. Khanna *et al.* suggested that the suppression of the S peak at 20 K shows smearing out of the M–I transition by the disorder.[11] On the other hand, they also claimed that a more disordered sample tends to show smaller S at 300 K. This is opposite to the present result (Fig. 5(b)). However, the δ and/or the period of iodine chains are unclear in the literature, while the present samples are considered to have almost the same δ as described in 3.1.

Although much more systematic studies are needed to reveal the relation among the δ, iodine-chain correlation and S, here we adopt the present result showing that the disorder increases the absolute S at room temperature when the δ is unchanged. If it is the case, TTT–I_3 would be an exceptional material whose S increases as σ does. Its mechanism is unclear, but when the iodine chains are more ordered, a resulting energy gap and thermally excited carriers will suppress the S if the contribution of electrons becomes relatively large.

As for the thermal conductivity, it is difficult to discuss the precise sample dependence due to the low accuracy of its absolute value. Nevertheless, we can expect that the sample dependence of the κ is negligible as compared with that of the σ as discussed in 3.4.

By comparing the sample dependence of the three transport properties, we conclude that, at room temperature, the increase in the zT and PF is mainly due to the increase in the σ, which is enhanced as the iodine chains are more uncorrelated.

4.2 Comparison with theoretical predictions

The theoretical predictions by Casian and Sanduleac[14,15] motivated the present study, but the experimental zT at 300 K is smaller by two orders of magnitude than the maximum theoretical values. It is, however, not surprising when we consider the condition giving such

large zT reaching 1–2. It should be emphasized that the calculated zT strongly depends on the filling of a quasi-one-dimensional band, which is varied through the chemical composition TTT:I_3^-.

In a tight-binding model, the energy bands are made of the highest-occupied molecular orbitals of TTT molecules, whose formal charge of +0.5 for the 2:1 composition corresponds to the 1/4-filled hole band. In this case, the calculated zT seems less than 0.1 in the literature;[14,15] it is reasonablly close to that observed in the present study as well as that reported by Huewe *et al.*[16] The remaining difference is attributed to the κ_{lat}, namely, Casian and Sanduleac adopted ~1 $\mathrm{W{\cdot}K^{-1}{\cdot}m^{-1}}$ in their calculations, while the present authors and Huewe *et al.* observed 2–3 $\mathrm{W{\cdot}K^{-1}{\cdot}m^{-1}}$.

On the other hand, the calculated zT of 1–2 is obtained for *e.g.* the 2:0.5 composition (1/8-filling of holes). This is mainly due to the larger S than 100 $\mu\mathrm{V{\cdot}K^{-1}}$ at such small hole concentrations. In addition, Casian and Sanduleac also discussed the effect of the sample quality introducing the carrier scattering by impurities. They claim that it results in the violation of the Wiedemann–Franz law and also enhances the zT by ~30%.[14,15,29] Note that the concept of the "quality" is different from the "disorder" of the iodine chains; they affect the σ in the opposite ways.

Namely, one can expect that the crystals with less iodine contents, giving larger S, and with less impurity contents, giving higher σ/κ, are favorable to increase the zT on the basis of the theory. Although the present study shows that not the S but the higher σ by the uncorrelated iodine chains enhances the zT, this is the result obtained for the samples with $\delta \sim 0$.

Thus, further studies are needed to find a way to reduce the δ below zero to compare the experimental and theoretical results with each other, while the composition of the crystals as grown in a nitrobenzene solution or in a gas phase varies only around 2:(1±0.1).[10,17] One possible way is heating crystals in vacuum. Actually, Kaminskii *et al.*[17] reported decrease in the δ from 0.10 to 0 by heating at 150 °C for four hours. It would be worth trying it at higher temperatures and/or for longer time to achieve a large minus value of δ.

4.3 Comparison with other organic conductors

As organic materials for thermoelectric applications, much attention seems to be paid for conductive polymers in these days. They are mechanically flexible and suit for mass production. To the authors knowledge, $zT = 0.42$ (room temperature) of PEDOT:PSS is the highest of the conductive polymers,[30] where PEDOT and PSS are the abbreviations

of poly(3,4-ethylenedioxythiophene) and poly(styrenesulfonate), respectively. The material also shows the high PF of about 470 μW·K^{-2}·m^{-1} at room temperature. Note that these zT and PF was obtained for a cuboid/block sample. On the other hand, Wei *et al.* studied the anisotropy of the transport properties of the thin-film PEDOT:PSS and obtained $zT \sim 0.0085$ and $PF \sim 24$ μW·K^{-2}·m^{-1} for the in-plane direction; and $zT \sim 1.6 \times 10^{-4}$ and $PF = 0.81$ μW·K^{-2}·m^{-1} for the through-plane direction, respectively.[31)]

As for single crystals of the molecular conductors, Huewe *et al.* reported the thermoelectric properties of p-type TTT–I_3 as mentioned above; and also those of n-type (DMe-DCNQI)$_2$Cu (DMe-DCNQI = 2,5-dimethyl-*N,N*'-dicyanoquinonediimine).[16)] Their results on TTT–I_3 are similar to those observed for A, while they adopted the 3ω method to measure the κ. Furthermore, Huewe *et al.* claimed that $zT \geq 0.15$ was observed for (DMe-DCNQI)$_2$Cu for $T \leq 40$ K.

Some of the present authors ever determined the zT of other molecular conductors with the τ-type molecular packing.[32,33)] Among them τ-(ETO-*R,R*-DMEDT-TTF)$_2$(AuBr$_2$)$_{1+y}$ showed the highest zT (0.044 at 190 K) of the τ-type conductors ever reported, where ETO-*R,R*-DMEDT-TTF is ethylenethiooxy-*R,R*-dmethylethylenedithio-tetrathiafulvalane).

Although the zT of the order of 0.03 is still small, much smaller zT is obtained for "conventional" molecular conductors, *e.g.*, $zT = 1.83\times10^{-4}$ for TTF–TCNQ[34)] and $zT = 3.6\times10^{-3}$ for (TMTSF)$_2$PF$_6$,[35)] respectively. The low zT of these materials is due to their low S usually associated with high σ. This shows importance of searching for the molecular conductors with high σ and fairly large S like TTT–I_3.

5. Conclusions

The electrical resistivity ρ, thermopower S and thermal conductivity κ were simultaneously measured for the three single crystals of quasi-one-dimensional conductor (TTT)$_2$I$_{3+\delta}$ to investigate the sample dependence of the dimensionless thermoelectric figure of merit zT and power factor PF. It was found that both the zT and PF show large sample dependence, even though all the samples have nearly stoichiometric composition of TTT:I_3^- ~ 2:1 ($\delta \sim 0$), which was estimated by the X-ray diffraction analysis.

The sample dependence of the zT and PF is mainly attributed to that of the σ, whose magnitude and temperature dependence change through the degree of correlation among the iodine chains. It was found that the zT changes from 0.01 to 0.03 at room temperature when the σ grows as the iodine chains become more uncorrelated or disordered. The PF is also the highest for the most disordered sample and its maximum value reaches 730 μW·K^{-2}·m^{-1} at

35 K. This is, to the authors' knowledge, the highest *PF* ever reported for organic conductors.

The present zT is reasonably close to that predicted for the stoichiometric composition, TTT:I_3^- = 2:1. To improve the zT to the unity, it is needed to realize the S greater than ~ 100 $\mu V \cdot K^{-1}$ at room temperature as calculated for a composition like TTT:I_3^- = 2:0.5. Although such a low iodine content is difficult to realize, the non-stoichiometric nature of TTT–I_3 and weak correlation among the iodine chains will pave the way to control its physical properties to an extent. This is very unusual and unique as a molecular-based organic conductor.

Acknowledgments

One of the authors (Yoshino) thanks Prof. Takehiko Mori at Tokyo Institute of Technology for providing the information on synthesis of TTT and for the helpful discussion on the thermoelectricity of organic conductors; Prof. Jens Pflaum and Dr. Alexander Steeger at Julius–Maximilian University of Würzburg for providing the information on their recent studies of $(TTT)_2I_{3+\delta}$ as well as for the helpful discussion about the measurements and physical properties of the material; and Prof. Anatolie Casian at Technical University of Moldova for the helpful discussion on their theoretical works about molecular thermoelectric materials.

Finally, Yoshino greatly thanks Dr. Salavat S. Khasanov at Institute of Solid State Physics RAS Chernogolovka for providing expertise on the X-ray diffraction analysis and structural properties of $(TTT)_2I_{3+\delta}$.

This work was supported by JSPS KAKENHI Grant Numbers JP25400380 (Yoshino), JP17H05153 and JP18K05260 (Nakano) as well as by the Kyoto University Foundation (Yamochi).

References

1) J. He and M. Tritt, Science **357**, eaak9997 (2017).

2) B. Hilti and C. W. Mayer, Helvetica Chimica Acta **61**, 501 (1978).

3) D. L. Smith and H. R. Luss, Acta Crystallogr. B **33**, 1744 (1977).

4) R. P. Shibaeva and V. F. Kaminskii, Kristallografiya, **23**, 499 (1978).

5) R. P. Shibaeva, Lecture Note in Physics **96**, Quasi One-Dimensional Conductors, Pt. 2, 167–187 (1979).

6) C. Lowe-Ma, R. Williams, and S. Samson, J. Chem. Phys. **74**, 1966 (1981).

7) L. C. Isett and E. A. Perez-Albuerne, Solid State Commun. **21**, 433 (1977).

8) G. Mihály, A. Jánossy, and G. Grüner, Solid State Commun. **22**, 771 (1977).

9) R. B. Somoano, S. P. S. Yen, V. Hadek, S. K. Khanna, M. Novotny, T. Datta, A. M. Hermann, and J. A. Woollam, Phys. Rev. B **17**, 2853 (1978).

10) P. Delhaes, J.-P. Manceau, C. Coulon, S. Flandrois, B. Hilti, and C. W. Mayer, Lecture Note in Physics **96**, Quasi One-Dimensional Conductors, Pt. 2, 324–334 (1979).

11) S. K. Khanna, S. P. S. Yen, R. B. Somoano, P. M. Chaikin, C. Lowe Ma, R. Williams, and S. Samson, Phys. Rev. B **19**, 655 (1979).

12) S. K. Khanna R. B. Sommoano, and P. M. Chaikin, Lecture Note in Physics **96**, Quasi One-Dimensional Conductors, Pt. 2, 202–207 (1979).

13) A. Casian, J. G. Stockholm, V. Dusciac, and V. Nicic, J. Nanoelectron. Optoelectron. **4**, 95 (2009).

14) A. Casian and I. Sanduleac, J. Electron Mater. **43**, 3740 (2014).

15) I. Sanduleac, A. Casian, and J. Pflaum, J. Nanoelectron. Optoelectron. **9**, 247 (2014).

16) F. Huewe, A. Steeger, K. Kostova, L. Burroughs, I. Bauer, P. Strohriegl, V. Dimitrov, S. Woodward, and J. Pflaum, Adv. Mater. 1605682 (2017).

17) V. F. Kaminskii, M. L. Khidekel, R. B. Lyubovskii, I. F. Shchegolev, R. P. Shibaeva, E. B. Yagubskii, A. V. Zvarykina, and G. L. Zvereva, Phys. Stat. Sol. **44**, 77 (1977).

18) S. K. Khanna, W. W. Fuller, G. Grüner, and P. M. Chaikin, Phys. Rev. B **24**, 2958 (1981).

19) S. Megtert, J. P. Pouget, and R. Comes, Ann. Ny. Acad. Sci. **313**, 234 (1978).

20) S. Megtert, J. P. Pouget, R. Comes, and R. Fourme, Lecture Note in Physics **96**, Quasi One-Dimensional Conductors, Pt. 2, 196–201 (1979).

21) See Section 1 of Supplemental Material to this paper.

22) See Section 2 of Supplemental Material to this paper.

23) R. W. Powell, C. Y. Ho, and P. E. Liley, NSRDS-NBS-8: "Thermal Conductivity of Selected Material"s (U. S. Department of Commerce, Springfield, VA, 1966).

24) H. Yoshino, G. C. Papavassiliou, and K. Murata, J. Therm. Anal. Calorim. **92**, 457 (2008).

25) Y. Iwasaki, H. Yoshino, N. Kuroda, K. Kikuchi, and K. Murata, J. Phys. Soc. Jpn. **84**, 054601 (2015).

26) L. C. Isett, Phys. Rev. B **18**, 439 (1978).

27) Y. S. Karimov, G. I. Zverova, and E. B. Yagubskii, JETP Lett. **25**, 254 (1977).

28) See Section 3 of Supplemental Material to this paper.

29) A. Casian, Phys. Rev. B **81**, 155415 (2010).

30) G. H. Kim, L. Shao, K. Zhang, and K. P. Pipe, Nature Mater. **12**, 719 (2013).

31) Q. Wei, M. Mukaida, K. Kirihara, and T. Ishida, ACS Macro Lett. **3**, 948 (2014).

32) H. Yoshino, H. Aizawa, K. Kuroki, G. C. Anyfantis, G. C. Papavassiliou, and K. Murata, Physica B **405**, S79 (2010).

33) H. Yoshino, H. Nakada, S. J. Krivickas, H. Mori, G. C. Anyfantis, G. C. Papavassiliou, and K. Murata, Phys. Status Solidi C **9**, 1193 (2012).

34) H. Itahara, M. Maesato, R. Asahi, H. Yamochi, and G. Saito, J. Electron. Mater. **38**, 1171 (2009).

35) H. Yoshino, G. C. Papavassiliou, and K. Murata, Synth. Met. **159**, 2387 (2009).

Supplemental Material: Disorder-Enhanced Dimensionless Thermoelectric Figure of Merit zT of Non-stoichiometric Organic Conductor $(TTT)_2I_{3+\delta}$ ($\delta \leq 0.1$)

Harukazu Yoshino[1]*, Akifumi Hasegawa[1], Natsuki Kuroda[1], Manabu Ishikawa[2], Rika Tanaka[3], Masatoshi Kozaki[1], Yoshiaki Nakano[2,4], Akihiro Otsuka[2,4], and Hideki Yamochi[2,4]

[1]*Graduate School of Science, Osaka City University, Sumiyoshi-ku, Osaka 558-8585, Japan*
[2]*Research Center for Low Temperature and Materials Sciences, Kyoto University, Sakyo-ku, Kyoto 606-8501, Japan*
[3]*Graduate School of Engineering, Osaka City University, Sumiyoshi-ku, Osaka 558-8585, Japan*
[4]*Graduate School of Science, Kyoto University, Sakyo-ku, Kyoto 606-8502, Japan*

1. Sample preparation

1.1 Donor synthesis

Tetrathiatetracene (TTT, Fig. S1) was synthesized from sulfur and tetracene (= naphthacene).

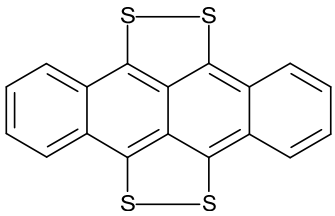

FIG. S1. Structural formula of TTT.

Sulfur (15 g) was solved in carbon disulfide (10 mL) below 40 °C. After filtering the solution to remove insoluble impurities, sulfur was recrystallized in the filtrate recovery at room temperature for 45 min; the precipitated crystals were aspirated. The light yellow sulfur crystals (7 g) were obtained after dried in a desiccator for 1 hour.

*yoshino@sci.osaka-cu.ac.jp

Tetracene (983.0 mg, > 97.0%, Tokyo Chemical Industry Co., Ltd.) and the sulfur obtained above (2.02 g) were solved in *N,N*-dimethylformamide (25 mL) within a 50-mL flask filled with nitrogen in advance. The solution was refluxed for 3.5 hours at 170 °C. The resulting dark blue solution was filtered before cooling; dark green TTT crystals were obtained. The crystals were washed with toluene and next with hexane; and dried in a desiccator. The dried crystals (1.42 g) was purified by sublimating at 1.3 Pa (0.01 Torr) and 230 °C. The dark green crystals of TTT (475.9 mg) were obtained with the yield of 31%.

1.2 Crystal growth

The crystal growth of $(TTT)_2I_{3+\delta}$ was carried out by the method similar to that in literatures.[1,2)]

TTT (17.6 mg) and iodine (11.2 mg) were solved in purified nitrobenzene (100 mL) at 100 °C so as to make each concentration about 5×10^{-4} mol L^{-1}. The hot solution (a in Fig. S2(a)) was poured into a crystal-growth glass cell (b). The cell had being capped (c) during the crystal growth; and placed inside a metal Dewar (d) with a Nichrome-wire heater (e), a platinum resistance thermometer (f) and a Chromel–Alumel thermocouple (g). The Dewar was covered with aluminum foil (h) before winding the wire heater for good thermal contact in advance. A rubber sheet (i) was placed at the inside bottom of the Dewar as a thermal insulator. The top of the cell was fixed with thick wire (j) not to touch the Dewar.

The cell was specially designed to have smaller diameter at lower and colder side. The temperature at the top and bottom of the cell was monitored with the thermometer and the thermocouple. The temperature difference was typically 10 °C during the crystal growth. It took 20 days to cool the solution from 100 °C to room temperature by controlling it with a PC to keep a constant cooling rate. Black needle-like crystals (Fig. S2(b)) grew inside bottom of the cell (k in Fig. S2(a)). The crystals were filtered and dried.

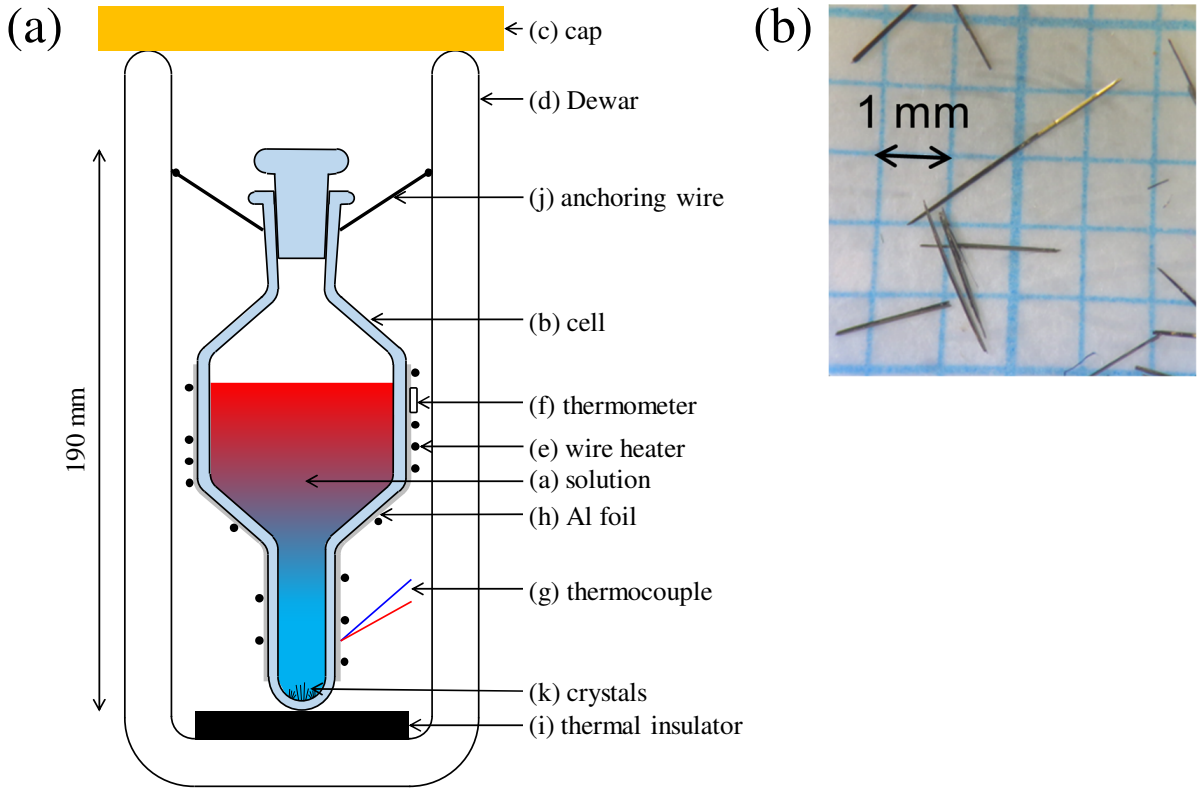

FIG. S2. (a) Schematic image of the crystal-growth cell of $(TTT)_2I_{3+\delta}$. (b) Single crystals of $(TTT)_2I_{3+\delta}$

2. Crystal structure

The obtained crystals were confirmed as $(TTT)_2I_{3+\delta}$ with the X-ray structural analysis on a single crystal. The crystal data are summarized in Table SI; and Fig. S3 shows the crystal structure viewed along each crystallographic axis. The TTT molecules and iodine atoms independently form chains along the ***b***-axis.

The structure was, however, not fully solved due to the existence of diffuse layers perpendicular to the ***b***-axis(Fig. S3). Thus the iodine atoms in Fig. S3 were tentatively placed and their positions along the ***b***-axis are not correct.

The existence of the diffuse layers shows that each of the iodine chains is regarded as an independent one-dimensional crystal and they are uncorrelated from one another. The

FIG. SI. Crystal data and structure refinement for $(TTT)_2I_{3+\delta}$.

Empirical formula	$C_{36}H_{16}I_3S_8$	
Formula weight	1085.67	
Temperature	296(2) K	
Wavelength	0.71075 Å	
Crystal system	Orthorhombic	
Space group	*Cmca*	
Unit cell dimensions	a = 18.3591(17) Å	$\alpha = 90°$
	b = 4.9715(4) Å	$\beta = 90°$
	c = 18.4275(17) Å	$\gamma = 90°$
Volume	1681.9(3) Å^3	
Z	2	
Density (calculated)	2.144 Mg/m^3	
Absorption coefficient	3.314 mm^{-1}	
$F(000)$	1038	
Crystal size	$0.350 \times 0.020 \times 0.010$ mm^3	
Theta range for data collection	4.389 to 27.493°	
Index ranges	$-23 \le h \le 22, -6 \le k \le 6, -23 \le l \le 23$	
Reflections collected	7985	
Independent reflections	993 [R(int) = 0.0304]	
Completeness to θ = 25.242°	99.2%	
Refinement method	Full-matrix least-squares on F^2	
Data / restraints / parameters	993 / 0 / 64	
Goodness-of-fit on F^2	1.128	
Final R indices [$I > 2\sigma(I)$]	$R1$ = 0.0503, $wR2$ = 0.1131	
R indices (all data)	$R1$ = 0.0557, $wR2$ = 0.1163	
Largest diff. peak and hole	1.328 and −0.819 e/Å^{-3}	

unit length of the idone chains along the ***b***-axis is determined as $b' \simeq 2b$ from the distance between the diffuse layers. The thickest layers are $k' = \pm 3$ (Fig. S4(a)). These features are reproduced by calculating the structure factor for the one-dimensional crystal composed of I_3^- units, whose I–I bond length and lattice parameter are 2.93 Å and $b' = 2b \sim 9.9$ Å, respectively.[4)]

On the other hand, the diffuse layers became subtle and new spots appeared at 100 K (Fig. S4(b)) indicating that the correlation among the iodine chains develops at lower temperatures.

Lowe-Ma *et al.* studied the low temperature crystal structure of highly-disordered (h.d) and least-disordered (l.d.) samples down to low temperatures.[4)] They pointed out the possibility that the unit cell of the l.d. sample is doubled as compared with the h.d. one. Although they claimed that there is no evidence for a structural phase transition between 19 and 294 K for the h.d. sample, the anomalies in the resistivity derivative and thermopower at 197 K observed for the samples A (#1602) and B (#1704) (Figs. 4(b) and 5(b) in the manuscript) imply that a kind of structural phase transition occurs at the temperature. Since these samples correspond to the medium-disordered crystal from the peak height of the thermopower at about 25 K,[5,6)] we cannot exclude a possibility that an ordering transition from the h.d.-like to l.d.-like structures occurs during the thermal contraction of the crystals. Similar behavior has been already reported by Megtert *et al.*[7)]

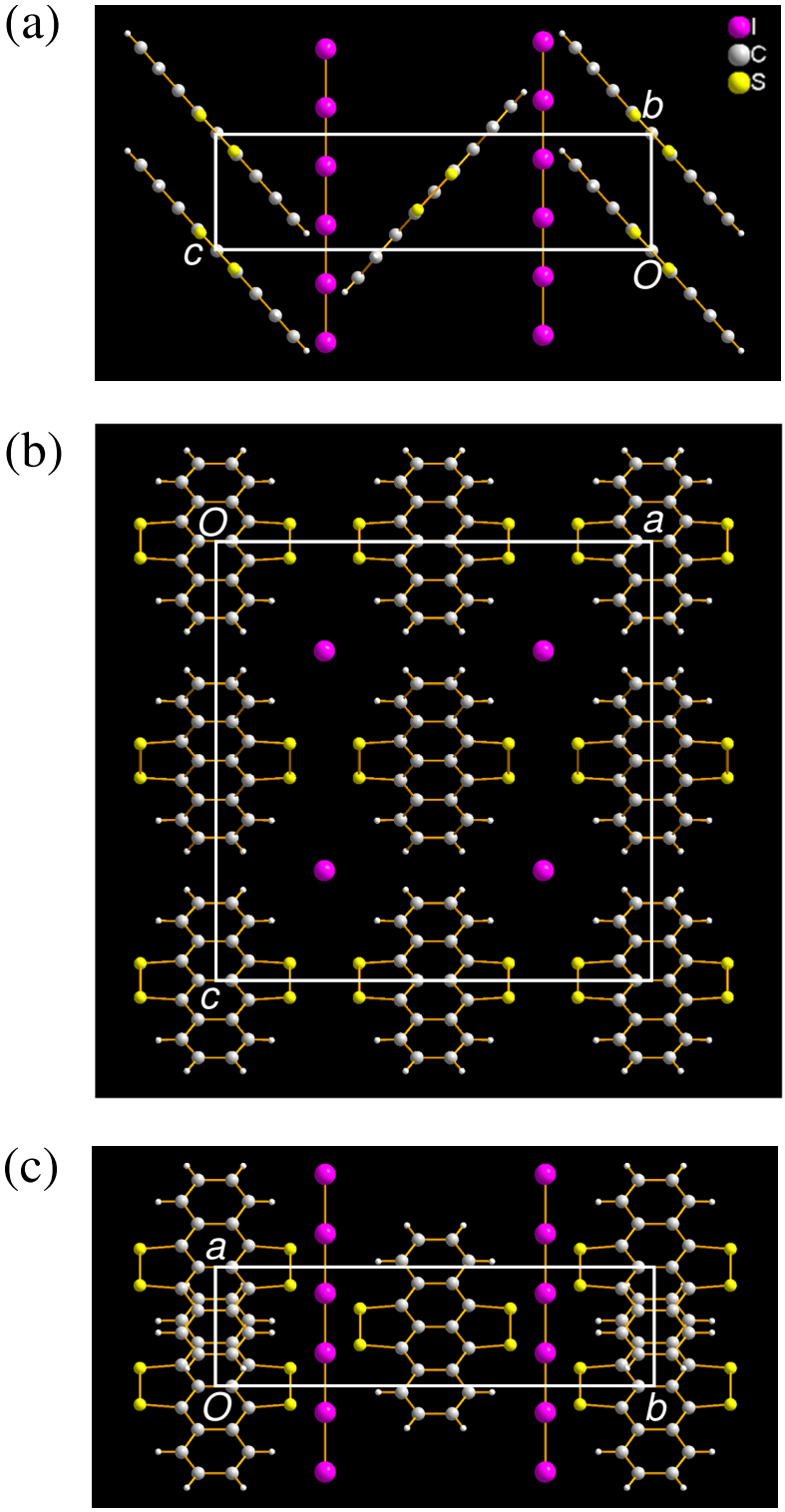

FIG. S3. Crystal structure of $(TTT)_2I_{3+\delta}$ viewed along the (a) ***a***-, (b) ***b*** and (c) ***c***-axes, respectively.

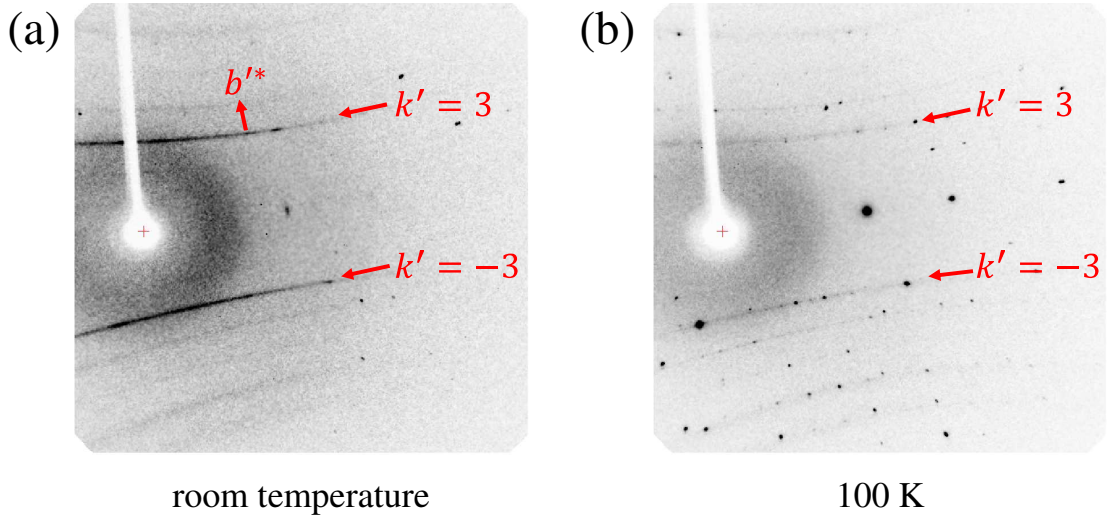

FIG. S4. X-ray photographs of $(TTT)_2I_{3+\delta}$ taken at (a) room temperature and (b) 100 K, respectively. The diffuse layers observed at room temperature became much thinner and new spots were observed at 100 K.

3. Electronic and lattice thermal conductivities

Here we tentatively separate the observed thermal conductivity $\kappa_{\rm tot}$ into the lattice $\kappa_{\rm lat}$ and electronic $\kappa_{\rm e}$ contributions as,

$$\kappa_{\rm tot} \quad = \quad \kappa_{\rm lat} + \kappa_{\rm e}. \tag{1}$$

We can use the $\sigma = 1/\rho$ — the ρ and $\kappa_{\rm tot}$ were simultaneously measured on the identical sample — to estimate the $\kappa_{\rm e}$ assuming that the Wiedemann–Franz law,

$$L \quad = \quad \frac{\kappa_{\rm e}}{\sigma T} \tag{2}$$

holds; and also that the Lorenz number L is a constant,

$$L \quad = \quad L_0 \ = \ 2.44 \times 10^{-8}\ {\rm W\,\Omega\,K^{-2}}, \tag{3}$$

though the L often depends on temperature.[8)]

Then the $\kappa_{\rm lat}$ is obtained by subtracting the $\kappa_{\rm e}$ from the measured $\kappa_{\rm tot}$. The results for the three samples are shown in Fig. S5. The result clearly shows that the lattice contribution is dominant in $(TTT)_2I_{3+\delta}$.

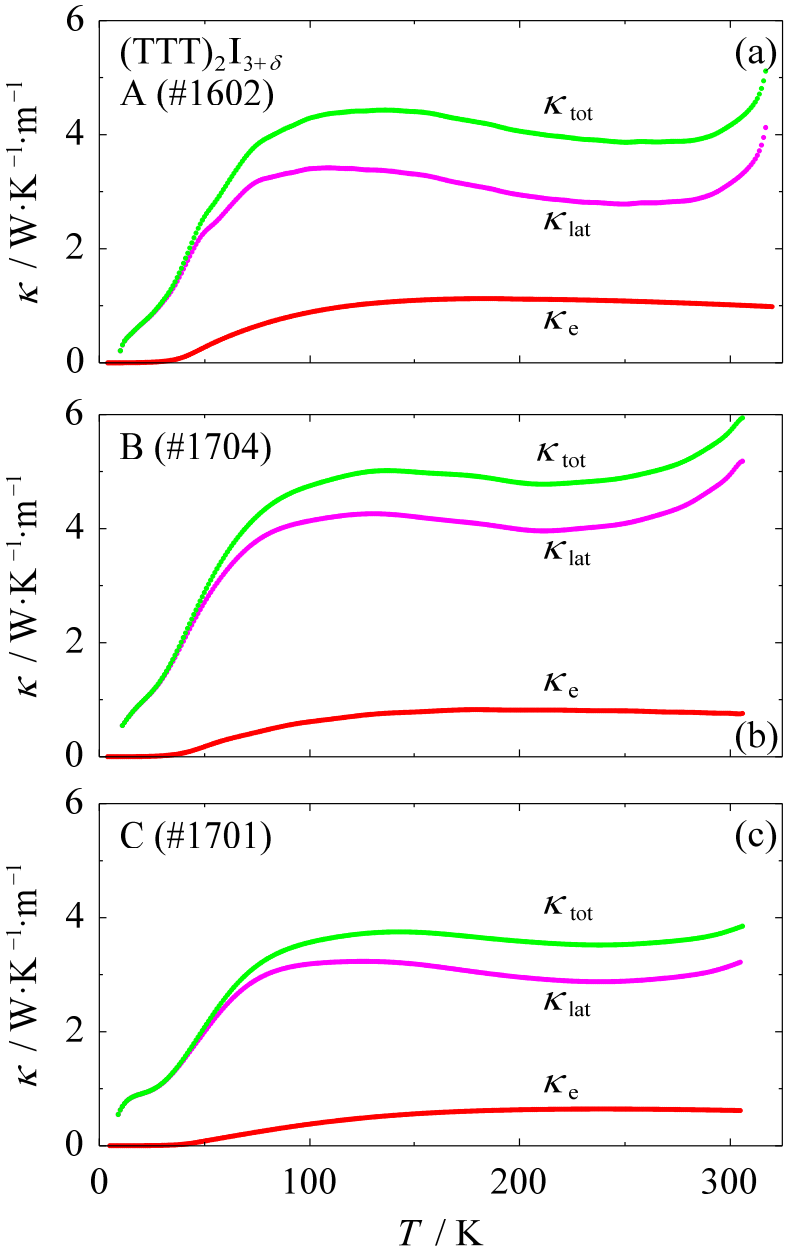

FIG. S5. Temperature dependence of the thermal conductivity κ_{tot} (green) of $(TTT)_2I_{3+\delta}$ measured for the samples (a) #1602, (b) #1701, and (c) #1704, respectively. The electronic contribution κ_e (red) was calculated from the resistivity assuming the Wiedemann–Franz law. The lattice contribution κ_{lat} (pink) was obtained by subtracting the κ_e from the κ_{tot}.

References

1) V. F. Kaminskii, M. L. Khidekel, R. B. Lyubovskii, I. F. Shchegolev, R. P. Shibaeva, E. B. Yagubskii, A. V. Zvarykina and G. L. Zvereva, Phys. Stat. Sol. **44**, 77 (1977).

2) G. Mihály, A. Jánossy, and G. Grüner, Solid State Commun. **22**, 771 (1977).

3) L. I. Buravov, G. I. Zvereva, V. F. Kaminskii, L. P. Rosenberg, M. L. Khidekel, R. P. Shibaeva, I. F. Shchegelov and E. B. Yagubskii, J. Chem. Soc. Chem. Commun. **18**, 720 (1976).

4) C. Lowe-Ma, R. Williams, and S. Samson, J. Chem. Phys. **74**, 1966 (1981).

5) S. K. Khanna, S. P. S. Yen, R. B. Somoano, P. M. Chaikin, C. Lowe Ma, R. Williams and S. Samson, Phys. Rev. B **19**, 655 (1979).

6) S. K. Khanna R. B. Sommoano and P. M. Chaikin, Lecture Note in Physics **96**, Quasi One-Dimensional Conductors, Pt. 2, 202–207 (1979).

7) S. Megtert, J. P. Pouget, R. Comes, and R. Fourme, Lecture Note in Physics **96**, Quasi One-Dimensional Conductors, Pt. 2, 196–201 (1979).

8) C. Uher, in *"Thermal Conductivity–Theory, Properties, and Applications"*, ed. T. M. Tritt (Kluwer Academic / Plenum, New York, 2004) p. 86.